



HAL
open science

Thermal characterization of polyethylene glycol 600 in liquid, solid phases and through the phase transition

Justine Noel, Yves Jannot, Christel Métivier, Nicolò R Sgreva

► **To cite this version:**

Justine Noel, Yves Jannot, Christel Métivier, Nicolò R Sgreva. Thermal characterization of polyethylene glycol 600 in liquid, solid phases and through the phase transition. 2021. hal-03516867v2

HAL Id: hal-03516867

<https://hal.science/hal-03516867v2>

Preprint submitted on 21 Mar 2022 (v2), last revised 29 Sep 2022 (v5)

HAL is a multi-disciplinary open access archive for the deposit and dissemination of scientific research documents, whether they are published or not. The documents may come from teaching and research institutions in France or abroad, or from public or private research centers.

L'archive ouverte pluridisciplinaire **HAL**, est destinée au dépôt et à la diffusion de documents scientifiques de niveau recherche, publiés ou non, émanant des établissements d'enseignement et de recherche français ou étrangers, des laboratoires publics ou privés.

Thermal characterization of polyethylene glycol 600 in liquid and solid phase and across the phase transition

Justine Noel^a, Yves Jannot^a, Christel Métivier^{a,*}, Nicolò R. Sgreva^a

^a*Université de Lorraine, LEMTA, CNRS, 54000 Nancy, France.*

Abstract

The polyethylene glycol (PEG) is characterized by experimental means in both solid and liquid phase. Main thermal properties inherent to the phase transition are also provided. More specifically, we focus on PEG 600, whose average molar mass is 600 g mol^{-1} and melting temperature transition is about 283-293 K. The phase change does not occur at a given temperature but rather over a range of temperatures, highlighting the complexity of the material. Several methodologies have been developed and calibrated in order to obtain, in both phases, the density and the thermal conductivity. A temperature dependence fit is proposed for the density in liquid phase. The relative density variation from the liquid to solid phase is significant as it can reach about 35 %, meaning a quite large volume shrinkage. Differential Scanning Calorimetry (DSC) has been used for measuring the heat capacity of solid and liquid phase and the effective heat capacity at the transition states. The latent heat of fusion and solidification converges to a value of around 130 kJ kg^{-1} . Undercooling effects are mitigated by performing DSC with slow temperature variation rates. Lastly, we have also observed several exothermic peaks during the solidification process that are related to structural reorganizations of the material.

1. Introduction

2 Polyethylene glycol (PEG) is a polyether present in our daily life and its
3 employment covers a wide range of industries, such as cosmetics, pharma-
4 ceuticals, food manufacturing, inks. As an example, it is used as a thickener

*christel.metivier@univ-lorraine.fr

5 agent in cosmetic products (liquid soaps, moisturizers, shampoos, etc.) and
6 paramedical products (hydro-alcoholic gels, intimate lubricants [1], etc.). It
7 is also used as a solvent in printer inks or to manufacture paint balls, as a
8 food additive and in certain polyester resins. Because it is a bio-compatible
9 product [2], it is also widely used in medical treatments and vaccines [3], as
10 recently for Covid-19 vaccine. In addition, the polyethylene glycol presents
11 remarkable properties: from a chemical viewpoint it is stable, non corro-
12 sive, non toxic. Another significant advantage lies in the large variety of
13 temperatures at which the solid/liquid transition occurs. Depending on
14 PEG's molecular weight, phase transition occurs for instance around 283-
15 293 K for PEG 600, 321-323 K for PEG 1000 [4] and around 324 K for PEG
16 1500 [5]. For these reasons, numerous studies have been devoted to propose
17 Composite Phase Change Materials (CPCMs) based on polyethylene glycol
18 [6, 7, 8, 9, 10, 11, 12]. Phase change materials (PCMs) are widely studied
19 in the field of energy storage/release since a large amount of energy can be
20 transferred during the phase change via latent heat. Energy is stored during
21 endothermic transformations (e.g. solid to liquid) while it is released dur-
22 ing exothermic transformations. The large latent heat of PEG makes it a
23 very interesting and attractive PCM. Furthermore, it matches perfectly the
24 criteria related to the choice of PCMs, such as being low-cost, non-toxic,
25 non-flammable, non-corrosive and biodegradable (bio-compatible), i.e. eco-
26 friendly. The uses of PEG in Composite PCMs can concern thermal reg-
27 ulation in buildings [13] or pavements [8] as well as in photovoltaic panels
28 [4, 12].

29 Despite the wide use of PEG, only few papers were devoted to characterize
30 the thermal properties of polyethylene glycol alone. Recently, Kou et al. [14]
31 have measured heat capacities of PEG for molar mass varying from 2000
32 to 20 000 g mol⁻¹. For smaller molar mass, as it is the case of PEG 600
33 (average molar mass of 600 g mol⁻¹), available data corresponds mainly to
34 properties for the liquid phase only. For instance, density measurements are
35 provided by several authors [15, 16, 17, 18], but they are given only for the
36 liquid phase and only for few temperature values, not sufficient to obtain the
37 thermal expansion coefficient. Some properties of PEG 600 are also given
38 by Lane [19]. This paper focuses on properties of PCMs; for PEG 600, the
39 author indicates the latent heat of melting and only one value for the melting
40 temperature. The thermal conductivity and the density in liquid phase are
41 provided for a couple of temperature values. Only some other studies present
42 the thermal conductivity of liquid phase, e.g. [17, 19]. Thus, properties of

43 PEG remain partially and scatteredly described in the literature. Moreover,
44 this small number of measured properties is obtained only for the liquid
45 phase. To our knowledge, the latent heat of solidification, the freezing point,
46 the thermal conductivity, the density and the heat capacity for the solid
47 phase are not available in the literature.

48 From a structural viewpoint, PEG's properties - in particular at the
49 solid/liquid transition - depend not only on the molecular weight but also
50 on the protocols involved in measuring them. Several types of aggregate
51 structures, such as helical or spherical conformations have been observed
52 within the freezing process [20, 21]. Understanding the correlation between
53 structural modifications and imposed experimental conditions is crucial since
54 the structural organization can have a significant impact on the macroscopic
55 properties. Indeed, in the case of semi-crystalline polymers as it is for PEG,
56 Bogdanov et al. [22] highlighted the influence of the cooling rate on the
57 exothermic crystallization peak by means of isothermal Differential Scan-
58 ning Calorimetry (DSC). Furthermore, a correlation between the heat flux
59 measurements obtained by DSC and the degree of crystallinity of PEG is
60 proposed by Pielichowski & Flejtuch [23].

61 As a first step in the understanding of the relationships between PEG's
62 behaviour and conditions of use, we clarify and provide new macroscopic
63 properties for PEG 600. The aim of our study is to characterize this polyether
64 in both the solid and liquid phase. In the liquid phase, we provide original
65 values of macroscopic properties and how they vary with temperature. In the
66 solid phase, we aim to fill the data gap in the literature. We carefully detail
67 the methodologies and protocols used to obtain the main thermal properties
68 in each phase (density, effective heat capacity and thermal conductivity) and
69 the latent heat of melting and solidification. In section 2, the different mea-
70 surement techniques and protocols used are detailed. Results are provided
71 in section 3 where they are also compared with the available literature. The
72 paper ends with conclusions and perspectives.

73 **2. Methods and experimental devices**

74 *2.1. Material*

75 Polyethylene glycol (PEG) is a linear polyether made from ethylene gly-
76 col monomers characterized by a molar mass generally smaller than 20 000
77 g mol^{-1} . In this study, we aim to characterize the polyethylene glycol with

78 molar mass of around 600 g mol^{-1} , named PEG 600. Several batches sup-
79 plied by Merck (CAS 25322-68-3) have been used to verify reproducibility of
80 results. The temperature of the solid-liquid phase change is indicated by the
81 supplier within the range of 290.15-293.15 K.

82 2.2. Density

83 2.2.1. Liquid phase

84 The density (ρ) of PEG 600 in liquid phase is measured by using a den-
85 simeter DMA 5000M, Anton Paar. The densimeter provides a $10^{-6} \text{ g cm}^{-3}$
86 accuracy in the temperature range of 273.15-333.15 K, while for larger tem-
87 peratures (up to a maximum of 373.15 K) the accuracy decreases to 10^{-4}
88 g cm^{-3} . The precision on the temperature is 0.01 K. Density measurements
89 are carried out at constant pressure P (atmospheric pressure) and at dif-
90 ferent temperature values within the range of 294.15-373.15 K where PEG
91 600 is liquid. Isothermal conditions are obtained by imposing temperature
92 steps with a 1 K increment in the range 294.15-323.15 K, followed by a 5 K
93 increment up to the temperature of 373.15 K. In the liquid phase, the time
94 to achieve the thermal stability is about 5 minutes per temperature step.

95 To ensure reproducible results, density is measured on three different sam-
96 ples (volume of $\sim 1 \text{ mL}$) from two different batches. At a given temperature,
97 the maximal variation between measurements is found to be $10^{-4} \text{ g cm}^{-3}$
98 and the final value of density is taken as the mean of these measurements.
99 From the temperature dependence of the density, we evaluate the thermal
100 expansion coefficient β as follows

$$\beta = -\frac{1}{\rho_{ref}} \left(\frac{\partial \rho}{\partial T} \right)_P, \quad (1)$$

101 with $\rho_{ref} = \rho(T_{ref})$ being a reference density defined at the temperature T_{ref} .
102 The thermal expansion coefficient indicates the first-order density variations
103 with temperature (Boussinesq approximation) at constant pressure [24] and,
104 for a given mass of a material, it also corresponds to the volume variation
105 with temperature.

106 2.2.2. Solid phase

107 Density measurements in the solid phase is achieved using a lab-made
108 pycnometer. This device is placed in a thermostatic enclosure BinderTM
109 KBF 115 in order to control the temperature. The pycnometer consists in

Table 1: Pressure measurements performed for the pycnometer calibration - Steps (1) and (2)

Step (1)			Step (2)		
P_i (bar)	P_f (bar)	P_f/P_i	P_i (bar)	P_f (bar)	P_f/P_i
3.654	1.685	46.1 %	3.655	2.002	54.7 %
3.660	1.696	46.3 %	3.650	2.002	54.8 %
3.665	1.706	46.5 %	3.603	1.976	54.8 %

110 two different cavities of volume V and V' separated by a valve as represented
 111 in Fig. 1. The measurement procedure is to initially obtain the vacuum in
 112 both cavities, i.e. $P' = P = 0$, then close the valve and impose a pressure P_i
 113 to the lower cavity. The valve is then opened involving pressure variations
 114 until an equilibrium is reached within the two cavities, leading to a final
 115 pressure P_f . The pressure is measured using a Mano 2000 Leo 3 Keller with
 116 an accuracy of 1 mbar

117 We first start by a calibration of the device, i.e. we determine the volumes
 118 V and V' of each cavity by repeating several times the above mentioned
 119 procedure through Steps (1) and (2) as indicated in Fig. 1 b. Volumes V
 120 and V' are determined via the following equation

$$P_i V = P_f \times (V + V' - V_{ref}), \quad (2)$$

121 where V_{ref} corresponds to the volume of a cylinder of height 0.02 m and
 122 radius 0.04 m. The procedure is repeated three times. Table 1 summarizes
 123 these measurements and shows the good stability in terms of pressure values
 124 (variation within 0.4 %).

125 Finally, Step (3) is performed with a given mass of PEG (Fig. 1 b).
 126 The temperature set in the binder is 273.75 K in order to have a fully solid
 127 sample. The volume of solid PEG is obtained using eq. (2) in which V_{ref} is
 128 replaced by the unknown sample volume. The density of PEG in solid phase
 129 is deduced from this measurement.

130 2.3. Thermal conductivity

131 2.3.1. Liquid phase

The thermal conductivity of the liquid phase is measured via the sta-
 tionary hot tube method [25, 26]. A sketch of the device developed in our
 laboratory is shown in Fig. 2. The sample is introduced in liquid phase into

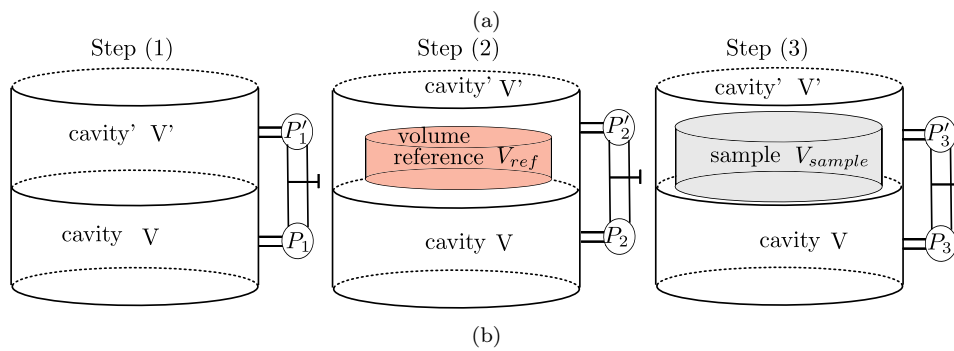


Figure 1: (a) Photo of the pycnometer and (b) sketch of the device through steps (1) and (2) used for the calibration of the device ; and step (3) used to measure the density of PEG 600 in solid phase.

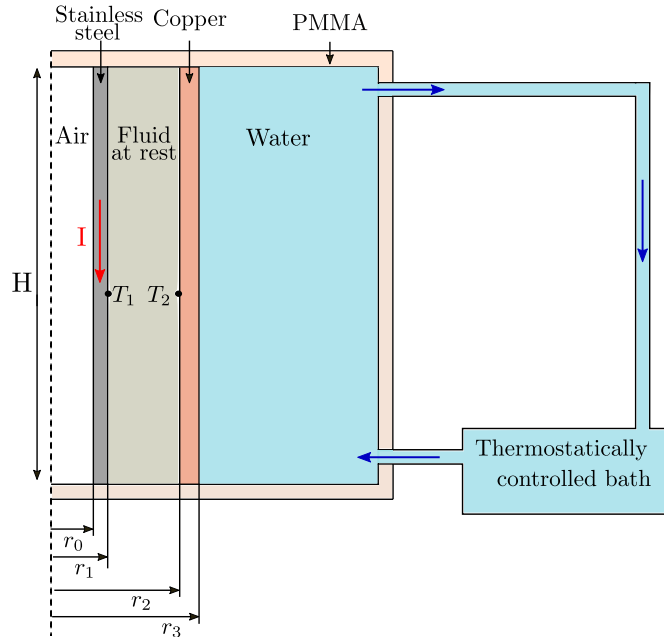


Figure 2: Sketch of the hot tube device used for thermal conductivity measurements. $r_0 = 2.54$ mm, $r_1 = 2.75$ mm, $r_2 = 6.00$ mm

the gap between two coaxial cylinders made of copper (the outer one) and stainless steel (the inner one). We ensure that the sample fills completely the space between the two cylinders, i.e. the space between r_1 and r_2 in Fig. 2. An electric current I is applied to the inner cylinder, producing heat flux by Joule effect. The outer part of the copper cylinder is maintained at a given temperature via a temperature controlled water flow. The temperatures T_1 and T_2 are measured using two type K thermocouples locked on the wall of the cylinders, i.e. at the boundaries of the liquid layer (as indicated in Fig. 2). Moreover, in order to avoid any up-down wall effects, thermocouples are located at the mid-height of the device. The temperature difference is measured thanks to the voltage difference U between these two thermocouples:

$$\Delta T = T_1 - T_2 = U/k,$$

132 where k is a constant equal to $k = (39.2 + 0.064 \times T_2 - 0.005 \times T_2^2) \times 10^{-6}$
 133 V K^{-1} . Thermocouples are connected to a cold junction block. Tension and
 134 electrical current are measured with a Keysight U3401A and an ISO-TECH
 135 IDM91E multimeter, respectively.

136 For a purely conductive regime in the liquid layer (fluid at rest), the
 137 thermal conductivity can be deduced as follows [25]:

$$\lambda = \frac{\rho_{el} I^2 \ln(r_2/r_1)}{2\pi^2(r_1^2 - r_0^2)\Delta T} \quad (3)$$

138 with $\rho_{el} = 7.3 \times 10^{-7}(1 + 1.36 \times 10^{-2}(T - T_{ref}))$ Ω m being the electrical
 139 resistivity of the stainless steel and T_{ref} a temperature reference equal to
 140 293.15 K.

141 The dimensions of the device are determined under the condition that no
 142 convection occurs for a wide range of fluids. According to [27], we ensure
 143 that the following condition is satisfied:

$$\frac{Ra}{H^+} < 400 \quad (4)$$

144 where $H^+ = H/\delta$, H is the height of cylinders, $\delta = r_2 - r_1$ is the thickness
 145 of the liquid layer and Ra corresponds to the Rayleigh number given by

$$Ra = \frac{\rho g \beta \Delta T \delta^3}{\mu a}, \quad (5)$$

146 with μ being the dynamic viscosity and a the thermal diffusivity of the
 147 fluid.

148 This condition is verified a posteriori and in the case of our measurements
 149 with PEG we estimate $Ra/H^+ \approx 15 - 20 \ll 400$.

150 Device validation performed with water leads to a maximal difference in
 151 thermal conductivity of 2 % with values provided by Brown & Marco [28]
 152 (i.e. a variation of $0.01 \text{ W m}^{-1} \text{ K}^{-1}$). Since the device is filled by the PCM
 153 in liquid phase, the volume of the sample varies with the temperature with a
 154 maximal variation occurring during the phase transition. As it is with most
 155 materials, PEG decreases in volume from liquid to solid phase. This can
 156 lead to imperfect contacts at walls during the solidification, as detailed in
 157 Appendix A. In this case, i.e. when thermal contact resistances are present
 158 at walls, the device becomes unsuitable for measuring thermal conductivity
 159 of materials in solid phase. For this reason, we propose another technique to
 160 carry out measurements in the solid phase. This technique is detailed in the
 161 following paragraph.

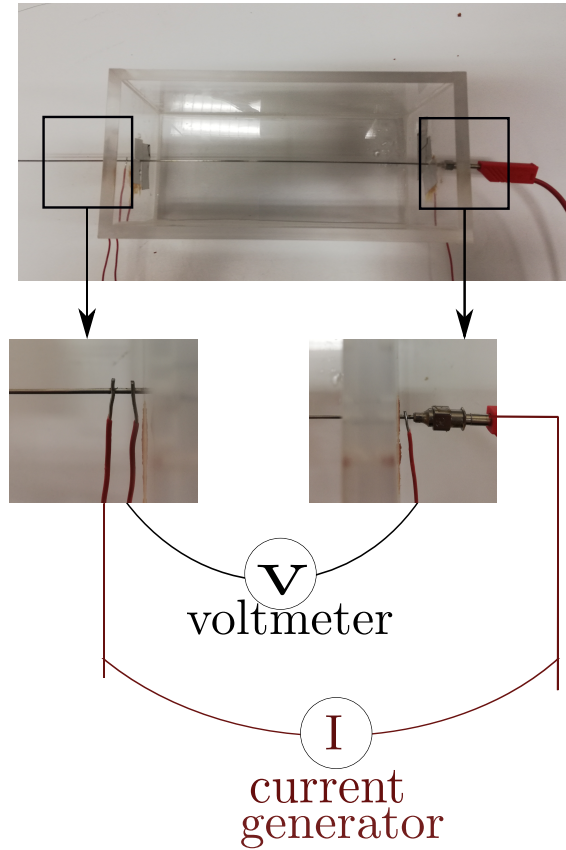


Figure 3: Photo of the heated needle device

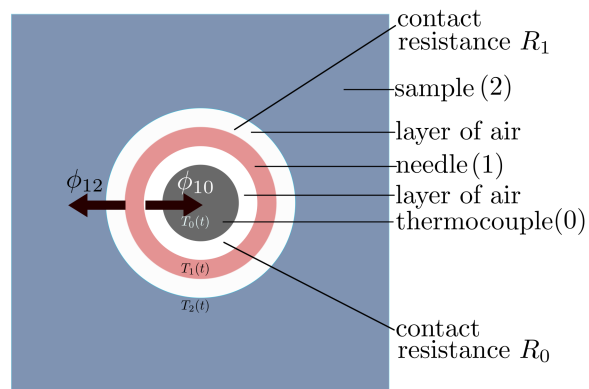


Figure 4: Schematic cross section of the hollow needle probe. The subscripts "0", "1" and "2" refer to the thermocouple, the needle and the sample, respectively.

162 *2.3.2. Hot needle method*

163 We developed a specific device in order to measure the thermal conductiv-
 164 ity of materials in solid or liquid phase. The device consists in a $200 \times 120 \times 120$
 165 mm^3 cavity made of PMMA that is filled with the sample.

166 A stainless steel hollow needle of length 300 mm is placed at the center
 167 of the device (Fig. 3). Needle's inner and outer radii are $r_i = 0.80$ mm and
 168 $r_e = 1.25$ mm, respectively. The needle is heated by Joule effect and the
 169 corresponding heat flow rate per unit of length L is $\phi = (UI)/L$, with U the
 170 electrical tension and I the electric intensity. Temperature is measured at the
 171 central point inside the needle with a K-type sheath thermocouple of radius
 172 $r_t = 0.5$ mm. Electrical tension and current are measured with a Tektronix
 173 DMM and an ISO-TECH IDM91E multimeter, respectively. Temperatures
 174 are recorded using a TC-08 Picolog device with a frequency of 10 Hz.

175 According to Fig. 4, in the following description we use the subscripts
 176 "0", "1" and "2" to refer to the thermocouple, the needle and the sample,
 177 respectively.

178 The device is placed in a BinderTM KBF 115 thermostatic chamber in
 179 order to maintain the system at a controlled temperature. The thermostatic
 180 chamber also guarantee a constant initial temperature $T(t = 0)$ in the whole
 181 system, i.e. $T_0(0) = T_1(0) = T_2(0)$, being the initial temperatures of the
 182 thermocouple, the needle and the sample, respectively. We assume uniform
 183 temperature field in the needle, $T_1(t)$, and in the thermocouple, $T_0(t)$, since
 184 they are very thin. Moreover, since contacts at interface 1-2, i.e. needle-
 185 sample, and at the interface 1-0, i.e. needle-thermocouple, are not perfect,
 186 also the thermal contact resistances R_1 and R_0 (see Fig. 4) have to be taken
 187 into account. Finally, due to the long length of the cavity, we consider an
 188 unidirectional dependence of parameters at the center of the cavity.

189 As the needle is heated, the total heat flow rate ϕ due to Joule effect can
 190 be split in two components, i.e. $\phi = \phi_{10} + \phi_{12}$ where ϕ_{12} is the heat transferred
 191 to the material and ϕ_{10} the heat transferred to the thermocouple. Heating
 192 the needle also induces transient variations in temperature within the whole
 193 system. Thermal properties of PEG can be obtained by considering the
 194 heat equation (conductive regime) in two domains assorted with boundary
 195 conditions. For this purpose, we use the quadrupole formalism proposed by
 196 Maillet *et al.* [29].

197 The first domain is bounded by the outer surface of the needle ($r_1 = r_e (\approx$
 198 $r_i)$) and a surface of the material sample ($r_2 \rightarrow \infty$). Following the method

199 proposed by Maillet [29], the thermal quadrupole formalism writes:

$$\begin{bmatrix} \theta_1 \\ \Phi_{12} \end{bmatrix} = [M1][M2] \begin{bmatrix} \theta_2 \\ \frac{\theta_2}{Z} \end{bmatrix} = \begin{bmatrix} 1 & 0 \\ C_1 p & 1 \end{bmatrix} \begin{bmatrix} 1 & R_1 \\ 0 & 1 \end{bmatrix} \begin{bmatrix} \theta_2 \\ \frac{\theta_2}{Z} \end{bmatrix} = \begin{bmatrix} 1 & R_1 \\ C_1 p & 1 + R_1 C_1 p \end{bmatrix} \begin{bmatrix} \theta_2 \\ \frac{\theta_2}{Z} \end{bmatrix} \quad (6)$$

with:

$\theta_1 = \mathcal{L}(T_1(t) - T_1(0))$ being the Laplace transform of the needle temperature variation $[T_1(t) - T_1(0)]$,

$\theta_2 = \mathcal{L}(T_2(t) - T_2(0))$ the Laplace transform of the material temperature variation at the interface needle/material $[T_2(t) - T_2(0)]$,

$\Phi_{12} = \mathcal{L}(\phi_{12})$ the Laplace transform of ϕ_{12} ,

$M1$ the quadrupolar matrix representing the needle as a pure capacity C_1 ,

$M2$ the quadrupolar matrix representing the contact resistance at the interface 1-2,

p the Laplace parameter (s^{-1}),

R_1 the thermal contact resistance per unit of length at the interface 1-2 ($m K W^{-1}$), and

$$C_1 = \pi(r_e^2 - r_i^2)\rho_1 c_1, \quad (7)$$

$$Z = \frac{K_0(qr_e)}{2\pi\lambda qr_e K_1(qr_e)}, \quad (8)$$

$$q = \sqrt{\frac{p}{a}} \quad (9)$$

200 where ρ_1 is the density of the needle ($kg m^{-3}$), c_1 the specific heat of the
 201 needle ($J K^{-1} kg^{-1}$), a the thermal diffusivity of the sample ($m^2 s^{-1}$), and λ
 202 the thermal conductivity of the sample ($W m^{-1} K^{-1}$).

203 Similarly, we consider a second domain that is bounded by the thermocou-
 204 ple $r_0 = 0 (\approx r_i)$ and the inner needle surface $r_1 = r_i (\approx r_e)$. The quadrupole
 205 formalism leads to:

$$\begin{bmatrix} \theta_1 \\ \Phi_{10} \end{bmatrix} = [M3][M4] \begin{bmatrix} \theta_0 \\ 0 \end{bmatrix} = \begin{bmatrix} 1 & R_0 \\ 0 & 1 \end{bmatrix} \begin{bmatrix} 1 & 0 \\ C_0 p & 1 \end{bmatrix} \begin{bmatrix} \theta_0 \\ 0 \end{bmatrix} = \begin{bmatrix} 1 + R_0 C_0 p & R_0 \\ C_0 p & 1 \end{bmatrix} \begin{bmatrix} \theta_0 \\ 0 \end{bmatrix} \quad (10)$$

206 with:

207 $\theta_0 = \mathcal{L}(T_0(t) - T_0(0))$ being the Laplace transform of the thermocouple tem-
 208 perature variation $[T_1(t) - T_1(0)]$,

209 $\Phi_{10} = \mathcal{L}(\phi_{10})$ the Laplace transform of the heat flow rate ϕ_{10} ,
 210 $M3$ the quadrupolar matrix representing the contact resistance at the inter-
 211 face 0-1,
 212 $M4$ the quadrupolar matrix representing the thermocouple as a pure capac-
 213 ity C_0 ,
 214 R_0 the thermal contact resistance per unit length between the thermocouple
 215 and the needle (m K W^{-1}), and

216

$$C_0 = \pi r_t^2 \rho_0 c_0 \quad (11)$$

217 where ρ_0 is the density of the thermocouple (kg m^{-3}) and c_0 the specific heat
 218 of the thermocouple ($\text{J K}^{-1} \text{kg}^{-1}$).

From Eq.(6) we deduce:

$$\theta_1 = \left(1 + \frac{R_1}{Z}\right) \theta_2, \quad (12)$$

$$\Phi_{12} = \left(C_1 p + \frac{1 + R_1 C_1 p}{Z}\right) \theta_2 = \left(C_1 p + \frac{1 + R_1 C_1 p}{Z}\right) \frac{\theta_1}{1 + \frac{R_1}{Z}}. \quad (13)$$

From Eq.(10) we deduce:

$$\theta_1 = (1 + R_0 C_0 p) \theta_0, \quad (14)$$

$$\Phi_{10} = C_0 p \theta_0 = \frac{C_0 p}{1 + R_0 C_0 p} \theta_1. \quad (15)$$

The Laplace transform of the total heat flow rate ϕ writes:

$$\mathcal{L}(\phi) = \frac{\phi}{p} = \Phi_{12} + \Phi_{10} = \left(\frac{Z C_1 p + 1 + R_1 C_1 p}{Z + R_1} + \frac{C_0 p}{1 + R_0 C_0 p}\right) \theta_1, \quad (16)$$

and by substituting Eq.(14) into Eq.(16) we obtain

$$\theta_0 = \frac{\phi}{p} \frac{Z + R_1}{(Z + R_1)[(C_0 + C_1)p + R_0 C_0 C_1 p^2] + 1 + R_0 C_0 p}. \quad (17)$$

At long time ($p \rightarrow 0$), the above equations simplify to:

$$\theta_0 = \frac{\phi}{p}(Z + R_1), \quad (18)$$

$$K_0(qr_e) = -\ln\left(\frac{qr_e}{2}\right) - \gamma, \quad (19)$$

$$K_1(qr_e) = \frac{1}{qr_e}, \quad (20)$$

$$\theta_0(p) = \frac{\phi}{p} \left[-\frac{\ln\left(\frac{qr_e}{2}\right)}{2\pi\lambda} - \frac{\gamma}{2\pi\lambda} + R_1 \right] \quad (21)$$

$$= \frac{\phi}{p} \left[-\frac{\ln(p)}{4\pi\lambda} - \frac{\ln\left(\frac{r_e}{2\sqrt{a}}\right)}{2\pi\lambda} - \frac{\gamma}{2\pi\lambda} + R_1 \right]. \quad (22)$$

By performing the inverse Laplace transform, we obtain:

$$T_0(t) = \phi \left[\frac{\ln(t)}{4\pi\lambda} + \frac{\gamma}{4\pi\lambda} - \frac{\ln\left(\frac{r_e}{2\sqrt{a}}\right)}{2\pi\lambda} - \frac{\gamma}{2\pi\lambda} + R_1 \right], \quad (23)$$

and finally

$$T_0(t) = \frac{\phi}{4\pi\lambda} \ln(t) + \phi \left(\frac{-\gamma}{4\pi\lambda} - \frac{\ln\left(\frac{r_e}{2\sqrt{a}}\right)}{2\pi\lambda} + R_1 \right). \quad (24)$$

219 Equation (24) highlights a logarithm dependence of T_0 with time that
 220 becomes the dominant term at long time. This equation is valid only if the
 221 regime remains conductive and the medium is infinite. Hence, we can write:

$$T_0(t) = D_1 + D_2 \times \ln(t) \quad (25)$$

222 with D_1 and D_2 being two constants which depend on the material's thermal
 223 conductivity λ . Temperature measurements allow us to identify these two
 224 parameters by minimizing $S = \sum_{t_d}^{t_f} (T_{\text{exp}}(t) - T_0(t))^2$ on a time interval $[t_d, t_f]$,

225 where T_{exp} is the experimental temperature measured by the thermocouple
 226 and T_0 the temperature obtained from Eq. (25). The thermal conductivity
 227 is finally obtained by evaluating the following equation:

$$\lambda = \frac{\phi}{4\pi D_2}. \quad (26)$$

228 At a given temperature, the experiments are repeated three times and the
 229 final value of conductivity is taken as the mean of these experiments. The
 230 maximum variation of λ obtained in this way is $0.01 \text{ W m}^{-1} \text{ K}^{-1}$.

231 *2.4. Specific heat capacity and latent heat*

232 The specific heat capacity c_p as well as the latent heat of the material are
 233 obtained using a Setaram μdSc3 differential calorimeter.

234 The protocol consists in applying temperature variations to the sample
 235 (sample mass about 200 - 300 mg) and in measuring simultaneously the
 236 heat transfer over time. In this present study, temperature variations are
 237 generated either through ramps of different rates of cooling/heating (1 K
 238 min^{-1} , 0.5 K min^{-1} , 0.2 K min^{-1}) or through temperature steps that lead to
 239 quasi-steady thermal conditions. In the latter case, steps last long enough in
 240 order to recover the steady state, i.e. no more heat flux between the sample
 241 and the device. In our experiments, this corresponds to a minimum of 1 hour
 242 up to 2 hours per temperature step. Increments between temperature steps
 243 are set to 1 K when phase change occurs, i.e. between 283.15 K and 303.15 K,
 244 to gain accuracy in evaluating the effective $c_p(T)$. Outside this temperature
 245 range, the increment is 2 K. The increment between two successive steps is
 246 obtained by applying a temperature ramp of 0.2 K min^{-1} .

247 Long steps or slow temperature variations have the advantage to avoid or
 248 at least to minimize undercooling effects. Reversibility of results are tested
 249 performing the entire protocol both increasing and decreasing the temper-
 250 ature. The effective heat capacity is deduced from the heat transferred to
 251 the sample after each temperature variation. At the phase transition, the
 252 equivalent c_p varies strongly due to the addition of latent heat to sensible
 253 heat. The latent heat is therefore estimated by subtracting the sensible heat
 254 obtained for the liquid or solid phase from the total heat measured at the
 255 phase change.

256 This protocol has been tested with pure water. The heat capacity mea-
 257 sured at 294.48 K is $4.125 \text{ kJ kg}^{-1} \text{ K}^{-1}$ for a reference value of $4.182 \text{ kJ kg}^{-1} \text{ K}^{-1}$.
 258 This leads to a difference of $0.057 \text{ kJ kg}^{-1} \text{ K}^{-1}$, i.e. a deviation of 1.4 %.

259 **3. Results**

260 *3.1. Density*

261 *3.1.1. Liquid phase*

262 Density measurements of PEG 600 are presented in Fig. 5 in the tem-
263 perature range of [294.15, 373.15] K. Measurements have been performed by
264 cooling the sample in order to avoid any issues related with the formation of
265 bubbles (that occurs when the material is heated over a large temperature
266 range) or with the presence of a mushy phase at the beginning of the analysis,
267 i.e. around 294.15 K. This precaution enables to obtain reproducible density
268 values under our experimental conditions.

269 Our experimental values are summarized in Fig. 5 together with values
270 currently present in literature [18, 15, 16]. We observe a very good agreement
271 between our results and literature (see also Table 2 where deviations are
272 shown). Our results are found within a maximum difference of 1% from
273 those reported in the above cited studies. Our results can be fitted by a
274 linear model (continuous line in Fig. 5) as follows:

$$\rho(T) = -8.1643 \times 10^{-4} T + 1.3652 \text{ g cm}^{-3}, \quad (27)$$

275 with T being the temperature in K. Furthermore, the thermal expansion
276 coefficient β can be evaluated according to Eq. (1). For instance, for $T_{ref} =$
277 298.15 K, we obtain $\rho_{ref} = 1.121956 \text{ g cm}^{-3}$ and $\beta = 7.28 \times 10^{-4} \text{ K}^{-1}$.

278 *3.1.2. Solid phase*

279 The density of PEG 600 in solid phase is obtained using the pycnometer
280 described in section 2.2.2. A material sample of around 150 g is placed in
281 the upper cavity of the pycnometer. The latter is left inside the thermostatic
282 chamber for 24 hours at temperature of 273.75 K. This is done before per-
283 forming any measurement in order to ensure the complete solidification of the
284 sample. Density measurements are afterward carried out at the same tem-
285 perature of 273.75 K by keeping the pycnometer with the solid sample inside
286 the thermostatic chamber for the entire duration of the experiment. Two
287 sets of pressure measurements are performed in each of which the measure-
288 ments are repeated 4 times (see Table 3). After the first set of measurement,
289 the sample is removed from the device and melted. The protocol is then
290 performed again for the second set.

291 For the range of PEG volume involved in our experiments, the error of
292 measurements is found smaller than 5%. This value is obtained using a

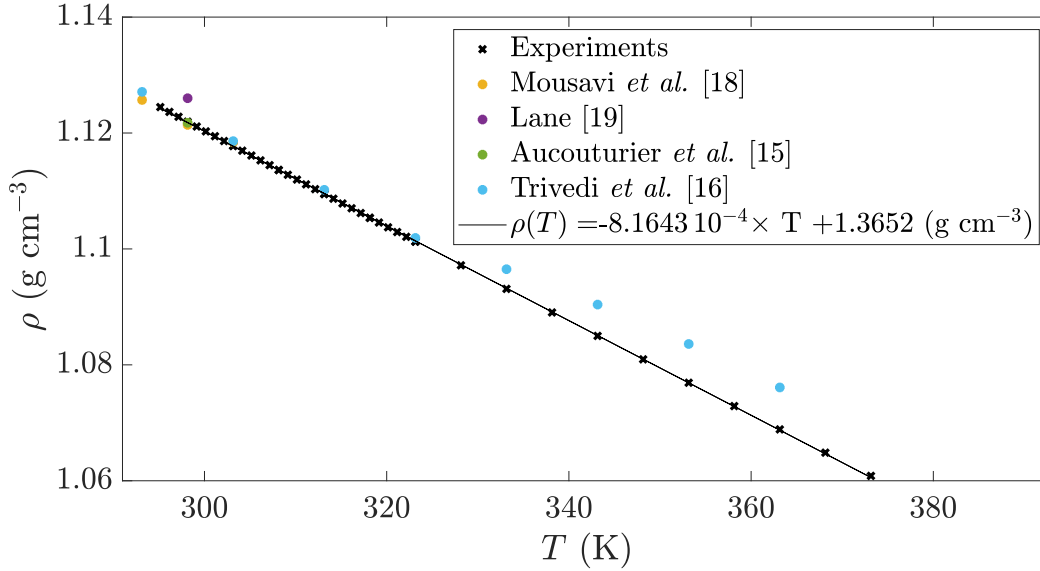


Figure 5: Density ρ of PEG 600 as a function of temperature.

Table 2: Comparison between some of our density measurements (ρ) of PEG 600 with values given in literature (ρ_{ref}).

T (K)	ρ (g cm ⁻³)	ρ_{ref} (g cm ⁻³)	Reference	Deviation (%)
298.15	1.121956	1.126	[19]	0.36
		1.1214	[18]	0.05
		1.12177	[15]	0.02
303.15	1.117763	1.1184	[18]	0.06
		1.1186	[16]	0.07
313.15	1.109468	1.1102	[16]	0.07
323.15	1.101259	1.1019	[16]	0.06
333.15	1.093104	1.0965	[16]	0.31
343.15	1.084992	1.0904	[16]	0.50
353.15	1.076914	1.0836	[16]	0.62
363.15	1.068864	1.0761	[16]	0.67

Table 3: Pressure measurements performed for one sample of PEG 600.

First set			Second set		
P_i (bar)	P_f (bar)	P_f/P_i	P_i (bar)	P_f (bar)	P_f/P_i
3.317	1.816	54.7 %	3.555	1.943	54.6 %
3.266	1.788	54.7 %	3.365	1.851	54.7 %
3.415	1.869	54.7 %	3.296	1.807	55.0 %
3.548	1.938	54.6 %	3.399	1.861	54.8 %

293 stainless steel sample with a known volume of $3.92 \times 10^{-5} \text{ m}^3$. The volume
 294 measured with the pycnometer led to $V_{sample} = 3.82 \times 10^{-5} \text{ m}^3$, i.e. within
 295 2.6 % difference with the real value.

296 The density of PEG 600 in solid phase is evaluated to $\rho = 1510 \pm 23 \text{ kg}$
 297 m^{-3} at 273.75 K, value that is quite different from the one obtained for the
 298 liquid phase. This is not surprising as it is correlated to the large variation
 299 in volume occurring during solidification.

300 3.2. Thermal conductivity

301 3.2.1. Liquid phase - Steady hot tube method

302 As above mentioned in section 2.3.1, the steady hot tube method is rel-
 303 evant only in the liquid phase as it requires good thermal contacts between
 304 the sample and the tubes surfaces. Since the device is filled with PEG 600
 305 in liquid phase, the largest decrease in volume that leads to thermal re-
 306 sistance at interfaces is observed at the liquid-to-solid transition. Above
 307 293.15 K, PEG 600 is liquid and we assume negligible surfaces contact re-
 308 sistance. Below this temperature, results are no longer reproducible due to
 309 the liquid-to-solid transition. Measurements are performed at steady state.
 310 Results obtained with this device are presented in Fig. 6 ('+' symbols) as
 311 a function of the mean temperature between the two thermocouples, i.e.
 312 $\bar{T} = T = (T_1 + T_2)/2$. Additional values of thermal conductivity given
 313 by Lane [19] and values from a data sheet provided by Dynalene [30] are
 314 also displayed in Fig. 6 for comparison. In our experiments the temperature
 315 variation $\Delta T = T_2 - T_1$ does not exceed 3 K through the annular region of
 316 the device, i.e. between r_1 and r_2 . In the range of the tested temperatures,
 317 we observe a slight temperature dependence of λ . These measurements are
 318 complemented by those obtained by using the hot needle method.

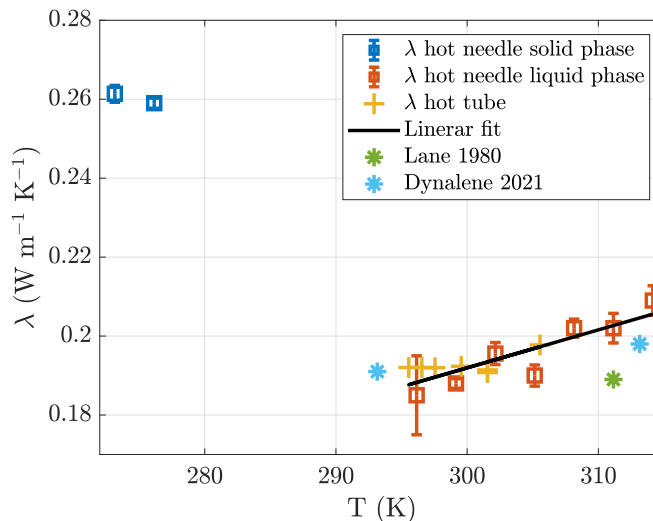


Figure 6: Thermal conductivity results for liquid phase and solid phases. Here the temperature T refers to the mean temperature between thermocouples, i.e. $T = \bar{T} = (T_1 + T_2)/2$.

3.2.2. Solid and liquid phases - Hot needle method

319 The measurements are carried out with the needle probe described pre-
 320 viously in Section 2.3.2. The estimation of the thermal conductivity λ is
 321 obtained assuming: (i) conductive regime in the vicinity of the needle, (ii)
 322 an infinite medium and (iii) $T(t) \propto \ln(t)$ at long time. The time interval
 323 $[t_i, t_f]$, in which the latter condition is satisfied, is determined empirically
 324 when the difference between experiments and the model is close to zero (see
 325 the discussion below about residuals).
 326

327 Thermal conductivity values in the solid phase are obtained placing the
 328 device in the temperature controlled binder. An example of temperature
 329 measurement is plotted in Fig. 7 as a function of time. In the same fig-
 330 ure we also display temperature values estimated by the model given by Eq.
 331 (25). Residuals multiplied by 10 times are also plotted in order to highlight
 332 the differences between measurements and the model. For each set of ex-
 333 periments, we determine the time interval $[t_i, t_f]$ along which residuals are
 334 perfectly flat and centered on zero, i.e. the time interval in which our model
 335 is consistent. This interval is bounded by vertical lines in Figs. 7 and 8. In
 336 the case presented in Fig. 7, the estimation time interval is $[20, 1000]$ s. The
 337 divergence of the residuals after 1000 s indicates the limit of validity of the
 338 infinite medium assumption. Following Eq. (25), we evaluate D_2 within the

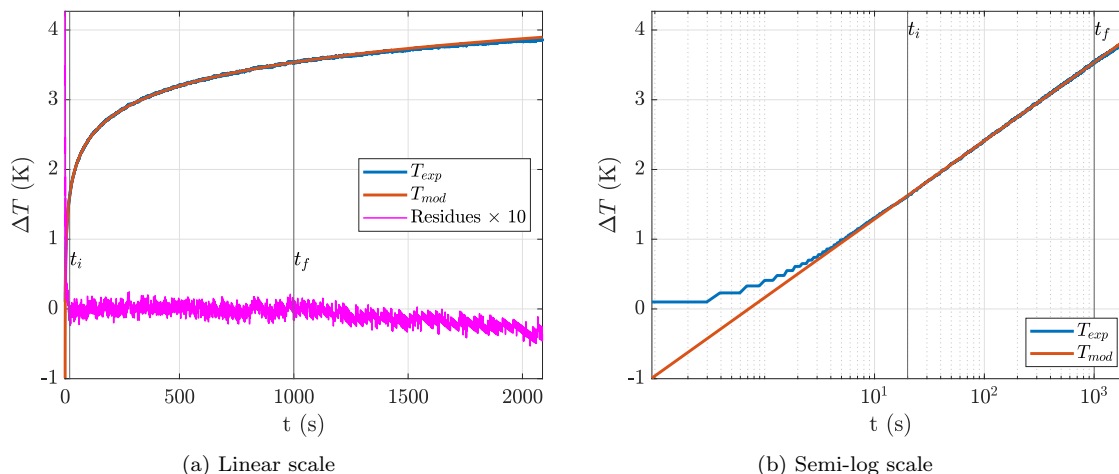


Figure 7: Experimental (T_{exp} , in blue) and simulated (T_{mod} , in red) curves for solid PEG 600 at 276.15 K obtained with the hot needle method. The red curve is obtained with the simplified model from Eq. (25). Magenta curve in (a) displays the residues S between T_{exp} and T_{mod} multiplied by 10 times.

339 estimation interval as the slope of the temperature variation with time in
 340 semi-log scale (Fig. 7b).

341 The model also applies to the liquid phase only if convection does not
 342 occur. For this reason, we have also performed some measurements above
 343 293.15 K. We show them in Fig. 8, where experimental and simulated tem-
 344 perature variations are displayed as a function of time. The same conditions
 345 described above are assumed and residuals are again plotted multiplied by
 346 10 times. Figure 8 corresponds to two different temperatures imposed in the
 347 chamber, i.e. 299.15 K and 314.15 K. The estimation interval was adjusted
 348 to $[50, 300]$ s for the measurement at 299.15 K and to $[20, 60]$ s for the
 349 measurement at 314.15 K. The residuals are found flat and centered on zero
 350 over these intervals. In the case of 314.15 K, the divergence of the residuals
 351 after 60 s is explained by the occurrence of convection around the needle.
 352 The higher the temperature is, the earlier this phenomenon appears. For
 353 instance, convection is not observed before 300 s for the case at 299.15 K.

354 Figure 6 summarizes all the thermal conductivity measurements as a function
 355 of temperature carried out for PEG 600. In liquid phase, values obtained
 356 via the needle method (squares) are consistent with the ones obtained using
 357 the hot tube method. The thermal conductivity in liquid phase shows
 358 a slight increase with increasing temperature following a linear variation:

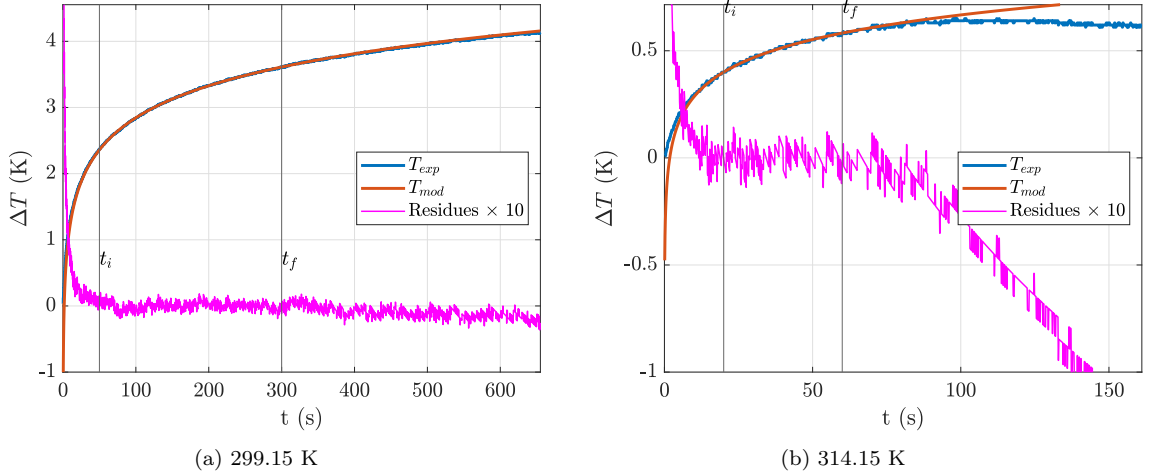


Figure 8: Experimental (T_{exp} , in blue) and simulated (T_{mod} , in red) curves for solid PEG 600 at 299.15 K (a) and 314.15 K (b) obtained with the hot needle method. The red curve is obtained with the simplified model from Eq. (25). Magenta curves display the residues between T_{exp} and T_{mod} multiplied by 10 times.

359 $\lambda(T) = 9.61 \times 10^{-4} T - 9.66 \times 10^{-2}$, with λ in $\text{W m}^{-1} \text{K}^{-1}$ and temperature
 360 T in K. Our results are also very close to those provided by Dynalene (see
 361 the data sheet in [30]), i.e. $\lambda = 0.191 \text{ W m}^{-1} \text{K}^{-1}$ at 293.15 K and $\lambda = 0.198$
 362 $\text{W m}^{-1} \text{K}^{-1}$ at 313.15 K. A good agreement is also found with values pub-
 363 lished by Lane [19], who obtained $\lambda = 0.189 \text{ W m}^{-1} \text{K}^{-1}$ at 311.00 K and
 364 $\lambda = 0.187 \text{ W m}^{-1} \text{K}^{-1}$ at 340.15 K.

365 In solid phase, the value of conductivity measured at 273.15 K and 276.15
 366 K does not vary much, leading to $\lambda_s \approx 0.260 \text{ W m}^{-1} \text{K}^{-1}$ in this temperature
 367 interval. However, for PEG 600 in solid phase it remains quite difficult to
 368 increase the range of temperatures. This is because, for a mean temperature
 369 of 279.15 K, the temperature near the needle is around 283.00 K and the
 370 material starts to melt. Hence, the gap between 276.15 K and 293.15 K in
 371 terms of thermal conductivity (Fig. 6) is explained by the occurrence of the
 372 phase transition.

373 To summarize, our measurements provide values of thermal conductivity
 374 in each liquid and solid phase. An effective value of λ in solid phase can
 375 be measured in the temperature range [276.15, 293.15] K. However we think
 376 that a careful investigation of the material structure at the phase transition
 377 would be more relevant. This aspect is beyond the scope of this present
 378 article but it will be investigated in the near future.

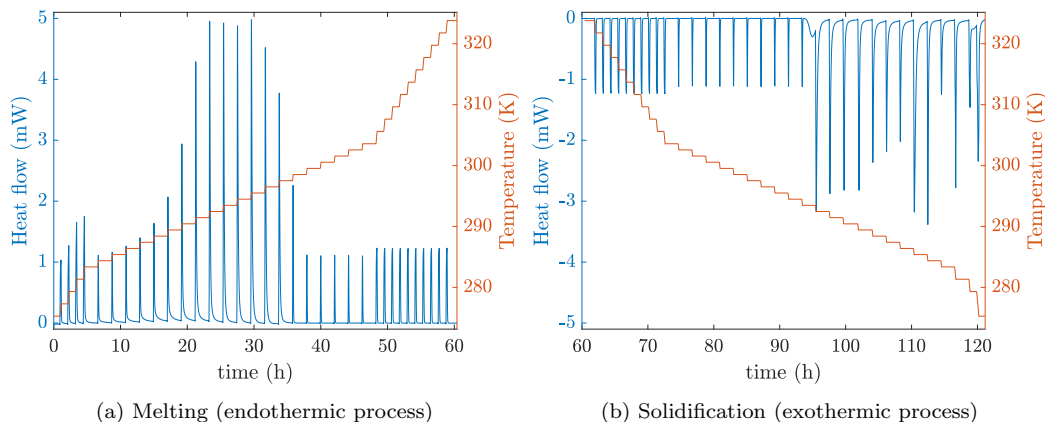


Figure 9: Heat flow rate measured from DSC (in blue) and imposed temperature steps (in red) as a function of time. (a) Melting of PEG 600 for increasing temperature steps (endothermic process). (b) Solidification of PEG 600 for decreasing temperature steps (exothermic process).

379 3.3. Specific heat capacity and latent heat

380 Raw data obtained by differential scanning calorimetry is presented in
 381 Fig. 9 for the case of imposed temperature steps (in red). The figure displays
 382 the amount of heat flux (in blue) transferred between the PCM sample and
 383 the calorimeter. Each increment of temperature leads to a peak in terms
 384 of heat exchanged. The latter goes back to zero as soon as the thermal
 385 equilibrium is reached. Given this experimental protocol, the effective heat
 386 capacity c_p is deduced by integrating the heat flux over the duration of a
 387 step (including the increment) and by dividing it by the mass of the sample
 388 m and the temperature increment.

389 On the other hand, if the protocol involves temperature ramps, i.e. con-
 390 tinuous temperature variations with time, we directly determine the effective
 391 c_p from the measured heat flux ϕ according to

$$\phi = mc_p \frac{dT}{dt}, \quad (28)$$

392 where the temperature variations rate $\frac{dT}{dt}$ is constant and imposed by the

393 ramp. We deduce then:

$$c_p = \frac{\phi}{m} \left(\frac{dT}{dt} \right)^{-1}. \quad (29)$$

394 The resulting values of effective c_p are shown in Fig. 10 as a function
395 of temperature. Similar trends are observed between the two protocols. For
396 large temperature values (above 298.15 K) the material is liquid and the heat
397 capacity is quasi constant, i.e. $c_p = 2.13 \text{ kJ kg}^{-1} \text{ K}^{-1}$. This value is recovered
398 in the liquid phase for both cooling and heating experiments.

399 Similarly, for low temperature values (below 283 K), the material is solid
400 and we obtain $c_p = 2.74 \text{ kJ kg}^{-1} \text{ K}^{-1}$.

401 In the temperature range where the phase transition occurs (i.e. solidifi-
402 cation in Fig. 10a and melting in Fig. 10b), variations in the evaluated c_p
403 are due to the competition between the kinetics of the phase change process
404 and the rate of temperature variations. This competition leads to a tempera-
405 ture hysteresis during solidification that corresponds to undercooling effects.
406 This latter phenomena decreases for slow temperature variations. In the case
407 of imposed temperature steps, the melting of PEG 600 is observed between
408 283.15 K and 295.15 K, while its solidification occurs between 293.15 K and
409 283.15 K. Further differences between melting and freezing processes can be
410 highlighted. Indeed, two distinct local maxima are observed during solidifi-
411 cation as the temperature decreases (Fig. 10a). These extrema are always
412 obtained for similar temperature values when the adopted cooling protocol
413 lasts long enough. Here, extrema correspond to exothermal transformations
414 correlated to structural modifications that occur during the crystallization
415 [20, 21]. Whatever the protocol used, the integration of only the part due to
416 the phase transition in the effective heat capacity leads to a latent heat of
417 130 kJ kg^{-1} . Reciprocally, at least one extrema value in terms of c_p is also ob-
418 tained for the melting process (Fig. 10b). When the heating process is long
419 enough (0.2 K min^{-1}), two local peaks are observed but their amplitudes are
420 smaller than in the case of the solidification process. These multiple peaks
421 are observed also in other studies that attribute them to microstructural vari-
422 ations i.e. crystals with different thickness due to variations in folds number
423 in the polymer chain [31] or due to the evolution of the lamellar microstruc-
424 ture during the phase change [32]. The latent heat is evaluated as previously
425 and values obtained from different protocols converge to 127 kJ kg^{-1} , which
426 is close to what obtained for the solidification process. Furthermore, our
427 values are in very good agreement with the one proposed by Lane [19], i.e.

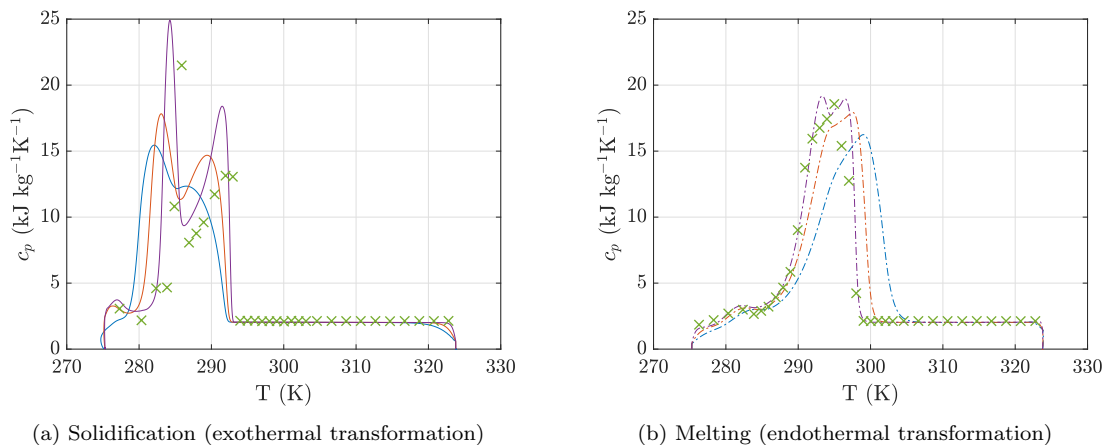


Figure 10: Effective $c_p(T)$ evaluated during (a) the solidification process and (b) the melting process, for temperature variations of 1 K min^{-1} (blue lines), 0.5 K min^{-1} (red lines), 0.2 K min^{-1} (purple lines) and temperature steps (green crosses).

428 127.2 kJ kg^{-1} .

429 4. Conclusion

430 In this study we report the thermal properties of polyethylene glycol 600
 431 (PEG 600). The density in liquid phase has been measured in the tempera-
 432 ture range $[298.15, 373.15] \text{ K}$. Given the small temperature increments used,
 433 we have been able to provide a fit for the temperature-dependent density of
 434 liquid PEG 600. The latter allows to determine the coefficient of thermal
 435 volume expansion with a good accuracy. The density of PEG 600 in solid
 436 phase has been measured by using a pycnometer and it results in $\rho = 1510$
 437 kg m^{-3} at 273.75 K . The variation of density between the two phases high-
 438 lights a quite large volume shrinkage of the material during solidification.
 439 This can have a drastic consequence on thermal contacts at interfaces and
 440 hence a strong impact in the usability of this PCM in thermal energy storage
 441 systems.

442 The thermal conductivity λ has been investigated with two different meth-
 443 ods. Results for the liquid phase show a slight linear increase of λ with in-
 444 creasing temperature, while for the solid phase we find $\lambda_s \approx 0.260 \text{ W m}^{-1} \text{ K}^{-1}$
 445 within the investigated temperature range.

446 Effective heat capacity and heat transfer have been described and quan-
 447 tified by DSC measurements. Far from the phase transition, we obtain a

448 constant specific heat capacity for both solid and liquid phase. The phase
449 transition occurs between 283.15 K and 298.15 K, depending whether the
450 sample is cooled or heated. Undercooling effects are responsible for the hys-
451 teresis in phase change temperature, however they decrease when the cooling
452 rate is decreased. For the different protocols tested in DSC, we obtain a sim-
453 ilar value for the latent heat, i.e. 130 kJ kg⁻¹. Furthermore, during the
454 solidification process we observe several exothermic peaks that highlight re-
455 organizations of aggregates and/or crystals in the internal structure of PEG
456 600. This latter aspect is beyond the scope of this study. However, since
457 explanations on PEG crystallization are still controversial in literature, a
458 proper investigation at small scales of this process will be a fundamental
459 part of our future work.

460 **Appendix A. Estimation of the error due to steady-state contact** 461 **resistances**

462 During solidification, the density of the sample increases and $\rho_l < \rho_s$, with
463 ρ_l being the density of the liquid phase and ρ_s the one of the solid phase.
464 This results in a decrease in volume with temperature. In the hot tube device
465 used to measure the thermal conductivity, this leads to an air/vacuum layer
466 of thickness ϵ between the sample and the inner heating tube of radius r_1
467 (Fig. 2).

468 One can write:

$$\rho_l \pi (r_2^2 - r_1^2) = \rho_s \pi [r_2^2 - (r_1 + \epsilon)^2], \quad (\text{A.1})$$

leading to

$$\epsilon = \left[r_2^2 - \frac{\rho_l}{\rho_s} (r_2^2 - r_1^2) \right]^{0.5} - r_1.$$

469 The thermal resistance between the two tubes is:

$$R = \frac{1}{2\pi\lambda} \ln \left(\frac{r_2}{r_2 - r_1 - \epsilon} \right) + \frac{1}{2\pi\lambda_{air}} \ln \left(\frac{r_1 + \epsilon}{r_1} \right) = \frac{1}{2\pi\lambda_m} \ln \left(\frac{r_2}{r_1} \right). \quad (\text{A.2})$$

470 In this way, λ_m is the measured value of the thermal conductivity while
471 λ is the real thermal conductivity of the solid sample. We deduce:

$$\lambda_m = \ln \left(\frac{r_2}{r_1} \right) \left[\frac{1}{\lambda} \ln \left(\frac{r_2}{r_2 - r_1 - \epsilon} \right) + \frac{1}{\lambda_{air}} \ln \left(\frac{r_1 + \epsilon}{r_1} \right) \right]^{-1}. \quad (\text{A.3})$$

472 The radii values are $r_1 = 2.75$ mm; $r_2 = 6$ mm. With an estimated
473 value for the thermal conductivity in solid phase of $\lambda = 0.26$ W m⁻¹ K⁻¹, we
474 can calculate the value λ_m that we would have measured with the hot tube
475 method. For $\rho_l/\rho_s = 0.75$, the calculation leads to $\lambda_m = 0.19$ W m⁻¹ K⁻¹, i.e.
476 around 30% less than the actual value. For this reason, the steady-state hot
477 tube device used in this study to measure λ of liquid PEG 600 is unsuitable
478 to retrieve λ of the solid phase. For measurements of thermal conductivity
479 of solid PCMs is therefore preferable to use a transient measurement device
480 where contact resistances have no influence on estimating the conductivity.

481 Acknowledgments

482 Financial supports have been brought to this work by the operation
483 “STOCK’NRJ” co-financed by the European Union within the framework
484 of the Program FEDER-FSE Lorraine and Massif des Vosges 2014-2020.

485 References

- 486 [1] M. Kobayashi, T. Koide, S.-H. Hyon, Tribological characteristics of
487 polyethylene glycol (PEG) as a lubricant for wear resistance of ultra-
488 high-molecular-weight polyethylene (UHMWPE) in artificial knee joint,
489 Journal of the Mechanical Behavior of Biomedical Materials 38 (2014)
490 33–38.
- 491 [2] K. Bjugstad, D. Redmond Jr, K. Lampe, D. Kern, J. Sladek Jr, M. Ma-
492 honey, Biocompatibility of PEG-based hydrogels in primate brain, Cell
493 Transplantation 17 (4) (2008) 409–415.
- 494 [3] A. K. Jain, A. K. Goyal, N. Mishra, B. Vaidya, S. Mangal, S. P. Vyas,
495 PEG–PLA–PEG block copolymeric nanoparticles for oral immunization
496 against hepatitis B, International Journal of Pharmaceutics 387 (1-2)
497 (2010) 253–262.
- 498 [4] S. M. Baygi, S. Sadrameli, Thermal management of photovoltaic so-
499 lar cells using polyethylene glycol 1000 (PEG1000) as a phase change
500 material, Thermal Science and Engineering Progress 5 (2018) 405–411.
- 501 [5] F. Hamad, E. Egelle, K. Cummings, P. Russell, Investigation of the
502 melting process of polyethylene glycol 1500 (PEG 1500) in a rectangular

- 503 enclosure, *International Journal of Heat and Mass Transfer* 114 (2017)
504 1234–1247.
- 505 [6] J. Wang, M. Yang, Y. Lu, Z. Jin, L. Tan, H. Gao, S. Fan, W. Dong,
506 G. Wang, Surface functionalization engineering driven crystallization
507 behavior of polyethylene glycol confined in mesoporous silica for shape-
508 stabilized phase change materials, *Nano Energy* 19 (2016) 78–87.
- 509 [7] J. Yang, E. Zhang, X. Li, Y. Zhang, J. Qu, Z.-Z. Yu, Cellulose/graphene
510 aerogel supported phase change composites with high thermal conduc-
511 tivity and good shape stability for thermal energy storage, *Carbon* 98
512 (2016) 50–57.
- 513 [8] J. Jin, F. Lin, R. Liu, T. Xiao, J. Zheng, G. Qian, H. Liu, P. Wen,
514 Preparation and thermal properties of mineral-supported polyethylene
515 glycol as form-stable composite phase change materials (CPCMs) used
516 in asphalt pavements, *Scientific Reports* 7 (1) (2017) 1–10.
- 517 [9] Y. Zhou, X. Liu, D. Sheng, C. Lin, F. Ji, L. Dong, S. Xu, H. Wu,
518 Y. Yang, Graphene oxide/polyurethane-based solid–solid phase change
519 materials with enhanced mechanical properties, *Thermochimica Acta*
520 658 (2017) 38–46.
- 521 [10] A. Sharma, V. V. Tyagi, C. Chen, D. Buddhi, Review on thermal energy
522 storage with phase change materials and applications, *Renewable and*
523 *Sustainable Energy Reviews* 13 (2) (2009) 318–345.
- 524 [11] B. Zalba, J. M. Marín, L. F. Cabeza, H. Mehling, Review on thermal
525 energy storage with phase change: materials, heat transfer analysis and
526 applications, *Applied Thermal Engineering* 23 (3) (2003) 251–283.
- 527 [12] M. Firoozzadeh, A. H. Shiravi, M. Shafiee, Experimental and ana-
528 lytical study on enhancing efficiency of the photovoltaic panels us-
529 ing Polyethylene-Glycol 600 (PEG 600) as a phase change mate-
530 rial, *Iranian Journal of Energy and Environment* 10 (2019) 23–32.
531 doi:10.5829/ijee.2019.10.01.04.
- 532 [13] R. Velraj, R. Seeniraj, B. Hafner, C. Faber, K. Schwarzer, Heat transfer
533 enhancement in a latent heat storage system, *Solar Energy* 65 (3) (1999)
534 171–180.

- 535 [14] Y. Kou, S. Wang, J. Luo, K. Sun, J. Zhang, Z. Tan, Q. Shi, Thermal
536 analysis and heat capacity study of polyethylene glycol (PEG) phase
537 change materials for thermal energy storage applications, *The Journal of*
538 *Chemical Thermodynamics* 128 (2019) 259–274.
- 539 [15] C. Aucouturier, G. Roux-Desgranges, A. Roux, Excess molar volumes
540 and excess molar heat capacities of (polyethylene glycols+ water) at
541 temperatures between $T=278$ K and $T=328$ K, *The Journal of Chemical*
542 *Thermodynamics* 31 (2) (1999) 289–300.
- 543 [16] S. Trivedi, C. Bhanot, S. Pandey, Densities of poly(ethylene glycol)+
544 water over the temperature range (283.15 to 363.15) K, *The Journal of*
545 *Chemical Thermodynamics* 42 (11) (2010) 1367–1371.
- 546 [17] A. Singh, R. Walvekar, M. Khalid, W. Y. Wong, T. Gupta, Thermo-
547 physical properties of glycerol and polyethylene glycol (PEG 600) based
548 DES, *Journal of Molecular Liquids* 252 (2018) 439–444.
- 549 [18] Z. Mousavi, M. Pirdashti, A. A. Rostami, E.-N. Dragoi, Thermophysical
550 properties analysis of poly (ethylene glycol) 600+ methanol, ethanol, 1-
551 propanol, and 2-propanol binary liquid mixtures, *International Journal of*
552 *Thermophysics* 41 (2) (2020) 1–26.
- 553 [19] G. A. Lane, Low temperature heat storage with phase change materials,
554 *International Journal of Ambient Energy* 1 (3) (1980) 155–168.
- 555 [20] L. Yang, T. Smith, Melting and solidification behavior of blends of high
556 density polyethylene with poly (butylene terephthalate), *Polymer Engi-*
557 *neering & Science* 33 (21) (1993) 1426–1430.
- 558 [21] A. Azri, P. Giamarchi, Y. Grohens, R. Olier, M. Privat, Polyethylene
559 glycol aggregates in water formed through hydrophobic helical struc-
560 tures, *Journal of Colloid and Interface Science* 379 (1) (2012) 14–19.
- 561 [22] B. Bogdanov, A. Vidts, E. Schacht, H. Berghmans, Isothermal crys-
562 tallization of poly (ϵ -caprolactone- ethylene glycol) block copolymers,
563 *Macromolecules* 32 (3) (1999) 726–731.
- 564 [23] K. Pielichowski, K. Flejtuch, Differential scanning calorimetry studies
565 on poly (ethylene glycol) with different molecular weights for thermal

- 566 energy storage materials, *Polymers for Advanced Technologies* 13 (10-
567 12) (2002) 690–696.
- 568 [24] D. D. Gray, A. Giorgini, The validity of the Boussinesq approximation
569 for liquids and gases, *International Journal of Heat and Mass Transfer*
570 19 (5) (1976) 545–551.
- 571 [25] Y. Jannot, A. Degiovanni, *Thermal properties measurement of materi-
572 als*, John Wiley & Sons, 2018.
- 573 [26] N. R. Sgreva, J. Noel, C. Metivier, P. Marchal, H. Chaynes, M. Isaiev,
574 Y. Jannot, Thermo-physical characterization of hexadecane during the
575 solid/liquid phase change, *Thermochimica Acta* (2022) 179 – 180.
- 576 [27] J. Huetz, J.-P. Petit, *Notions de transfert thermique par convection*,
577 *Techniques de l'Ingénieur (A1504A)* (Aug. 1990).
- 578 [28] A. I. Brown, S. M. Marco, *Introduction to heat transfer*, 3rd Edition,
579 Mc Graw-Hill Book Company, New York, 1958.
- 580 [29] D. Maillet, S. Andre, J. C. Batsale, A. Degiovanni, C. Moyne, *Ther-
581 mal quadrupoles: solving the heat equation through integral transforms*,
582 Wiley-Blackwell, 2000.
- 583 [30] Dynalene Inc., PEG Series: Techincal data sheet,
584 [https://www.dynalene.com/product-category/heat-transfer-
585 fluids/polyethylene-glycol-heat-transfer-fluids/](https://www.dynalene.com/product-category/heat-transfer-fluids/polyethylene-glycol-heat-transfer-fluids/).
- 586 [31] B. Wunderlich, *Macromolecular physics: Crystal nucleation, Growth,
587 Annealing 2* (1976).
- 588 [32] M. S. Lisowski, Q. Liu, J. Cho, J. Runt, F. Yeh, B. S. Hsiao, Crystalliza-
589 tion behavior of poly (ethylene oxide) and its blends using time-resolved
590 wide-and small-angle X-ray scattering, *Macromolecules* 33 (13) (2000)
591 4842–4849.